

Electromagnetic Scattering Analysis for Two-Dimensional Gaussian Rough Surfaces with Texture Characteristics Using Small-Slope Approximation Method

Rong-Qing Sun^{*}, Jing Xie, and Yang-Wei Zhang

Abstract—This paper is aimed at analyzing the electromagnetic (EM) scattering from the two-dimensional (2-D) Gaussian rough surfaces characterized by textures. Visual appearances of the stripe texture can be generated through the angle rotating in Fourier transform when the ratio of the correlation lengths in two directions is large enough. The scattering field is derived in Cartesian coordinate system through the small-slope approximation (SSA) method with plane incident wave. The normalized co-polarized radar cross section (NRCS) from 2-D Gaussian rough surface characterized by textures is calculated. In particular, several numerical results show the influences of incident angle, texture angle, correlation length, and root-mean-square height on the scattering from the textured rough surface. Finally, the validity of the SSA method is verified by comparisons of theoretical value and measured data.

1. INTRODUCTION

Research on the electromagnetic (EM) scattering from random rough surfaces is widely employed in the fields of globe remote sensing, sea research, surface detection and radar imaging [1–3]. In actual application, the data of EM scattering are mainly from practical measurement and theoretical deduction. For practical measurement, it is necessary to put in a lot of manpower and material resources in an aggressive environment. However, the theory model [4, 5], which is from theoretical deduction and makes comparison with experimental data, has some advantages, such as simple realization method, weak environment impact, which are extremely valuable in application. At present, there are two major kinds of scattering theories of rough surfaces, i.e., numerical method and approximate method. Numerical method has very high calculation precision but is more complicated and difficult to be realized. In this case, it is of the necessity to appeal to the approximate method. In the analysis of approximate theory, the classical methods include Kirchhoff approximation (KA), small perturbation method (SPM) and two-scale method (TSM) which combines KA with SPM [6–9]. Concerning KA, tangential plane approximation forms its basis, in which the curvature radii of rough surface are much larger than incident wave length so that the hypothesis of EM wave incident on the infinite plane tangential to a point on the rough surface is hold. In other words, the KA method is appropriate for large scale of rough surface but out of place for low grazing incidence, whereas SPM is suitable for a slightly rough surface [10]. Due to the respective application ranges of both KA and SPM based on statistical models of rough surfaces, there exists very great limitation. Further, TSM has extended the applied area of scattering of rough surfaces, but its defect lies in that the concept of the cutoff wave number, whose determination is lack of scientific basis, is introduced to distinguish between large-scale and small-scale rough surfaces when being calculated. For this reason, it is necessary to find a theory that can accurately solve EM scattering of rough surfaces without considering their structures. In this case, there appeared to be

Received 1 August 2015, Accepted 23 October 2015, Scheduled 29 October 2015

^{*} Corresponding author: Rong-Qing Sun (sunrongqing@126.com).

The authors are with the Aerospace Research Institute of Materials and Processing Technology, Beijing 100076, China.

relevant numerical methods, including extended boundary condition method (EBCM), Monte Carlo method (MCM), finite difference time domain method (FDTD) and approximate method SSA [11–14]. Among them, SSA is an effective calculation method and applied to any wavelengths and rough surfaces, and it is a more precise approximate method in which the expressions of different orders deduced are obtained by retaining the term number of the series expansions and can be degenerated into the results of KA and SPM in certain condition.

In recent years, a series of research results have been obtained in the statistical models of EM scattering from rough surfaces [15]. Johnson and Warnick [16], in detail, compared geometric optics (GO) with physical optics (PO) in the area of EM scattering theory of the rough surface with exponential correlation features and confirmed the effective conditions of PO through the comparison of the calculation results with accurate solutions. Hu et al. [17] compared and discussed the effects of RMS height and correlation length of rough surface on the effective conditions of several approximation methods. Additionally, some scholars performed research on deterministic model of EM scattering from random rough surface. Li and Xu [18] studied scattering and Doppler spectral analysis for 2-D linear and nonlinear sea surfaces by the SSA method.

Texture characteristics can reflect image properties and visual rough degree of rough surface in the remote sensing images [19, 20]. They are obtained by analyzing the stripe pattern distributed in the regular or irregular ways. So the texture characteristics are the foundation to describe and recognize images in both theory and application. The distinct texture characteristics are displayed in sandbank, cordillera and sea wave. Currently, the research on texture properties is mainly from the literature of radar image, but study of the EM scattering for textures is much less. Prakash et al. [21] only studied the variation of the specular scattering as soil textures at X band. So there is the necessity that the relation between EM scattering and Gaussian rough surface with texture properties is established.

The remainder of this paper is organized as follows. In Section 2, formulation for 2-D Gaussian rough surface, whose texture angles are adjustable, is briefly presented through the angle rotation in Fourier transform, and discrete analysis on the rough surface is performed. In Section 3, how the EM scattering calculations are carried out by using the first-order SSA (SSA-I) and second-order SSA (SSA-II) method is addressed. As the SSA method is an approximate theory based on the expansion of the surface slope, the second-order SSA will give a more accurate prediction of the scattering problems, especially for cross-polarization cases. In Section 4, the impacts of the scattering angles, incident angles, texture angles, RMS heights and correlation length on the single and average bistatic NRCS and the backscattering coefficient are discussed.

2. REALIZATION OF 2-D GAUSSIAN ROUGH SURFACES WITH TEXTURE

The linear filter method, which combines finite impulse response filtering (FIR) with fast fourier transform (FFT), is adopted to simulate 2-D rough surfaces [22].

2.1. Geometric Modeling of 2-D Gaussian Rough Surfaces

For a rough surface of the size of $L_x \times L_y$, the profile is formed by means of the periodic extension in the directions of x and y , respectively. Let $f(x, y)$ be the height at any location (x, y) , then use 2-D Fourier extension to act on it, i.e.,

$$f(x, y) = \frac{1}{L_x L_y} \sum_{m=-\infty}^{\infty} \sum_{n=-\infty}^{\infty} a_{mn} \exp \left(\frac{i2\pi m}{L_x} x + \frac{i2\pi n}{L_y} y \right) \quad (1)$$

where a_{mn} is complex amplitude of texture wave and Gaussian random variable [23]. Let $k_{mx} = 2\pi m/L_x$, $k_{ny} = 2\pi n/L_y$. Due to Fourier sum of Gaussian variable, $f(x, y)$ also obviously submits to Gaussian distribution. To obtain surface correlation function, we construct the functions as follows:

$$\begin{aligned} \langle f(x_1, y_1) f(x_2, y_2) \rangle &= \frac{1}{L_x^2 L_y^2} \sum_{m_1=-\infty}^{\infty} \sum_{n_1=-\infty}^{\infty} \sum_{m_2=-\infty}^{\infty} \sum_{n_2=-\infty}^{\infty} \langle a_{m_1 n_1} a_{m_2 n_2}^* \rangle \\ &\quad \exp \left[\frac{i2\pi}{L_x} (m_1 x_1 - m_2 x_2) + \frac{i2\pi}{L_y} (n_1 y_1 - n_2 y_2) \right] \end{aligned} \quad (2)$$

To satisfy the requirement of Gaussian power spectrum,

$$\begin{aligned}\langle f(x_1, y_1)f(x_2, y_2) \rangle &= \sigma^2 C(x_1 - x_2, y_1 - y_2) \\ &= \int_{k_x=-\infty}^{\infty} \int_{k_y=-\infty}^{\infty} dk_x dk_y \exp(ik_x(x_1 - x_2) + ik_y(y_1 - y_2)) W_G(k_x, k_y)\end{aligned}\quad (3)$$

where σ is the RMS height, $C(x_1 - x_2, y_1 - y_2)$ the correlation function which describes the coherence between different points on the surface separated by the distance between the point (x_1, y_1) and (x_2, y_2) , and $W_G(k_x, k_y)$ the corresponding power spectral density function (PDF) of surface. Comparing Eq. (2) with Eq. (3), we find that the quadruple summation series of Eq. (2) can be associated with Kronecker delta function, then is simplified as double summation. Correspondingly, spatial wave numbers in integral variables are discretized. The above processes can be expressed as follows [24, 25]:

$$\langle a_{m_1 n_1} a_{m_2 n_2}^* \rangle = \delta_{m_1 - m_2, n_1 - n_2} A_{m_1 n_1} \quad (4)$$

$$dk_x = \Delta k_x = \frac{2\pi}{L_x}, \quad dk_y = \Delta k_y = \frac{2\pi}{L_y} \quad (5)$$

$$k_x = m\Delta k_x, \quad k_y = n\Delta k_y \quad (6)$$

In this case,

$$\begin{aligned}& \frac{1}{L_x^2 L_y^2} \sum_{m=-\infty}^{\infty} \sum_{n=-\infty}^{\infty} A_{mn} \exp(ik_x(x_1 - x_2) + ik_y(y_1 - y_2)) \\ &= \frac{(2\pi)^2}{L_x^2 L_y^2} \sum_{m=-\infty}^{\infty} \sum_{n=-\infty}^{\infty} W_G(k_x, k_y) \exp(ik_x(x_1 - x_2) + ik_y(y_1 - y_2)) \\ &\Rightarrow A_{mn} = \langle a_{mn} a_{mn}^* \rangle = \langle |a_{mn}|^2 \rangle = (2\pi)^2 L_x L_y W_G(k_x, k_y)\end{aligned}\quad (7)$$

which gives the condition which module $|a_{mn}|$ satisfies. However, for complex coefficient a_{mn} , next step will discuss the satisfied relation between the real and imaginary parts of a_{mn} . To generate a real sequence, the requirement for $F(K_x, K_y)$ is that $F(K_x, K_y) = F^*(-K_x, -K_y)$ and $F(K_x, -K_y) = F^*(-K_x, K_y)$. At the same time, a_{mn} is inverse Fourier transform of $f(x, y)$. So it holds that

$$a_{mn} = a_{(-m)(-n)}^* \quad (8)$$

Further, due to the effect of Kronecker delta function in Eq. (4), let $m_2 = -m_1 = m$, $n_2 = -n_1 = -n$, i.e.,

$$\langle a_{mn} a_{(-m)(-n)}^* \rangle = \langle a_{mn} a_{mn} \rangle = 0. \quad (9)$$

which describes the relation complex coefficient a_{mn} as follows:

$$\begin{aligned}\langle [\text{Re}(a_{mn})]^2 \rangle &= \langle [\text{Im}(a_{mn})]^2 \rangle \\ \langle [\text{Re}(a_{mn})] \text{Im}(a_{mn}) \rangle &= 0\end{aligned}\quad (10)$$

Namely, $\text{Re}(a_{mn})$ and $\text{Im}(a_{mn})$ are independent Gaussian random variables, and their variances are both a half of $\langle |a_{mn}|^2 \rangle$. Additionally, Eq. (8) is combined with the periodic characteristics of a_{mn} , and we obtain the relation

$$a_{(-\frac{Nl}{2})(-\frac{Nl}{2})} = a_{\frac{Nl}{2} \frac{Nl}{2}}^* = a_{(-\frac{Nl}{2})(-\frac{Nl}{2})}^* \Rightarrow a_{(\frac{Nl}{2})(\frac{Nl}{2})} \in R. \quad (11)$$

At this point we obtain the real and imaginary parts of a_{mn} through the Gaussian distribution function which forms complex coefficient $G(m, n)$. Eventually, complex amplitude $a_{mn}(t)$ satisfying the above relations can be expressed by:

$$a_{mn}(k_{mx}, k_{ny}) = G(m, n) 2\pi \sqrt{L_x L_y W_G(k_{mx}, k_{ny})} + G^*(-m, -n) 2\pi \sqrt{L_x L_y W_G(k_{mx}, k_{ny})} \quad (12)$$

Through Eq. (1), the height value of $f(x, y)$ of rough surface can be generated by the FFT method.

This paper adopts Gaussian correlation function and Gaussian PDF to generate 2-D Gaussian rough surfaces, i.e.,

$$C(\tau_x, \tau_y) = \sigma^2 \exp\left(-\frac{\tau_x^2}{l_x^2} - \frac{\tau_y^2}{l_y^2}\right) \quad (13)$$

$$W_G(k_x, k_y) = \frac{l_x l_y \sigma^2}{4\pi} \exp\left(-\frac{k_x^2 l_x^2}{4} - \frac{k_y^2 l_y^2}{4}\right) \quad (14)$$

where τ_x and τ_y describe the separation between any two points along the x and y directions. The correlation length of the surface profiles is given by l_x and l_y . The surface is isotropic if $l_x = l_y$ and anisotropic if $l_x \neq l_y$. The power spectral density function of the surface $W_G(k_x, k_y)$ is related to the correlation function via a 2-D Fourier transform.

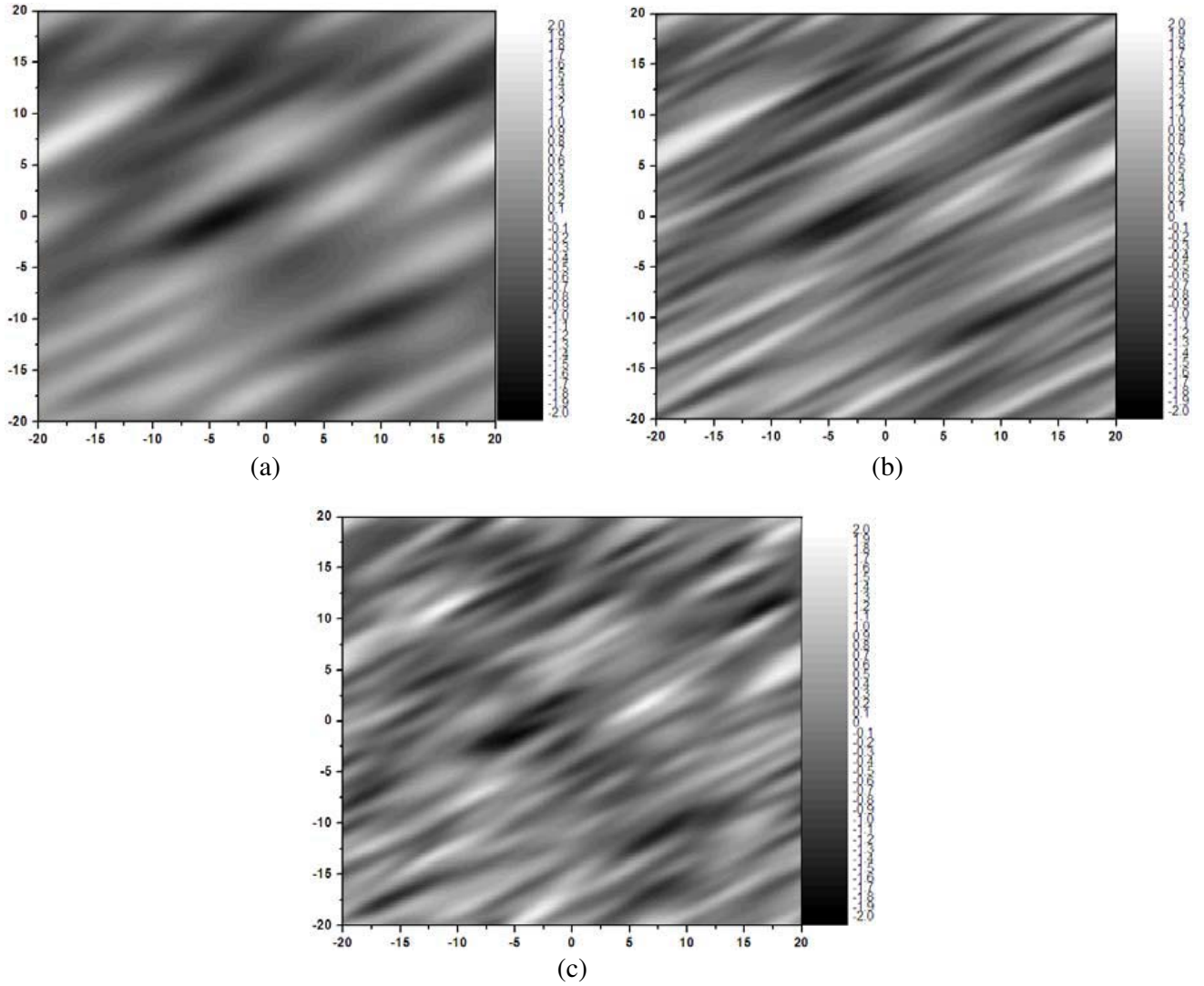


Figure 1. The simulated 2-D Gaussian rough surfaces with texture characteristics: (a) $l_x = 10$ m, $l_y = 2$ m, $\sigma = 0.6$ m. (b) $l_x = 10$ m, $l_y = 1$ m, $\sigma = 0.6$ m. (c) $l_x = 5$ m, $l_y = 1$ m, $\sigma = 0.6$ m. Texture angle is 30° .

2.2. Realizations of 2-D Gaussian Rough Surfaces with Texture

As this paper is aimed at the statistically anisotropic rough surfaces, we empirically limited the ratio of the l_x/l_y to be larger than 4, which guarantees that the surface can present a more anisotropic characteristic. Texture angle ϕ is defined as the angle between x -axis positive direction and texture direction. $W_G(k_{0x}, k_{0y})$ can be obtained through angle rotation action of the rotation matrix on Eq. (14), i.e.,

$$\begin{bmatrix} k_{0x} \\ k_{0y} \end{bmatrix} = \begin{bmatrix} \cos \phi & \sin \phi \\ -\sin \phi & \cos \phi \end{bmatrix} \cdot \begin{bmatrix} k_x \\ k_y \end{bmatrix} \quad (15)$$

Under this circumstance, the 2-D Gaussian rough surface by the FFT method also develops corresponding angle rotation.

The size of the simulated rough surface is 40×40 m, and there are 1024 sampling points in x and y directions. The simulated results are shown in Figure 1. Among them, (a) shows the simulation result, in which the RMS height σ is 0.6 m, correlation length l_x 10 m, l_y 2 m and texture angle ϕ 30° . Based on the above parameters, (b) changes l_y into 1 m, and (c) changes l_x into 5 m and l_y into 1 m. From Figure 1, we clearly find that the textures from (b) become narrower than that from (c), and the height variations from (c) become much more obvious than that from (b).

3. SCATTERING THEORY FROM ROUGH SURFACE BY SSA

In SSA, the geometrical configuration adopted to resolve the wave-scattering problem from the 2-D randomly rough surface is illustrated in Figure 2, where we consider a rough interface $z = h(\vec{r})$, with $\vec{r} = (x, y)$, between two homogenous half-spaces with permittivity ε_1 (upper half-space, $z > 0$) and ε_2 (lower half-space, $z < 0$) [26, 27]. The time dependence is assumed to be $\exp(-i\omega t)$. θ_i and θ_s are, respectively, incident and scattering elevation angles, and ϕ_i and ϕ_s are the incident and scattering azimuth angles, respectively. The incident wave vector can be expressed as $\vec{K}_i = \vec{k}_0 - q_0 \hat{z}$, where \vec{k}_0 and $-q_0$ are horizontal and vertical projections of the incident wave vector, respectively. The scattered wave vector is $\vec{K}_s = \vec{k} + q \hat{z}$, where \vec{k} and q are appropriate components of the scattered wave vector, respectively. q_0 and q can be expressed as $q_0 = \sqrt{\omega^2/c^2 - k_0^2}$, $q = \sqrt{\omega^2/c^2 - k^2}$, $\text{Im } q_0, q \geq 0$ [28].

The unit vector in the direction of incidence is:

$$\hat{K}_i = \sin \theta_i \cos \phi_i \hat{x} + \sin \theta_i \sin \phi_i \hat{y} - \cos \theta_i \hat{z} \quad (16)$$

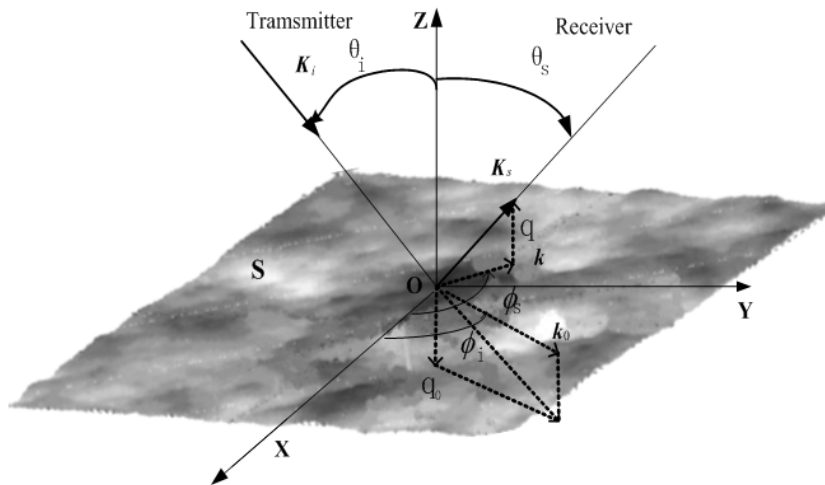


Figure 2. Geometry configuration for the wave scattering from 2-D surface.

and the incident wave vector $\vec{K}_i = K_i \hat{K}_i = (\vec{k}_0, -q_0)$. The incident field can be expressed as:

$$\begin{aligned}\psi_{inc}(\vec{R}) &= \exp(-i\vec{K}_i \cdot \vec{R}) = \exp[i(\vec{k}_0 \cdot \vec{r} - iq_0 z)] \\ &= \exp[-iK_i(z \cos \theta_i - x \sin \theta_i \cos \phi_i - y \sin \theta_i \sin \phi_i)]\end{aligned}\quad (17)$$

where $\vec{R} = (\vec{r}, q_0) = (x, y, z)$ and ψ_{inc} is electric field E or magnetic field H depending on the polarization.

The unit vector in the direction of scattering is:

$$\hat{K}_s = \sin \theta_s \cos \phi_s \hat{x} + \sin \theta_s \sin \phi_s \hat{y} + \cos \theta_s \hat{z} \quad (18)$$

and the scattered wave vector is $\vec{K}_s = K_s \hat{K}_s = (\vec{k}, q)$. The scattered field can be expressed as:

$$\psi_{sc}(x, y, z) = \int \exp(i\vec{k} \cdot \vec{r} + iqz) \bar{S}(\vec{k}, \vec{k}_0) d\vec{k} \quad (19)$$

Considering the case of far-field approximation, the scattering amplitude matrix corresponding to the SSA method can be modified as

$$\begin{aligned}\bar{S}(\vec{k}, \vec{k}_0) &= \frac{2(qq_0)^{1/2}}{\sqrt{P_{inc}}(q + q_0)} \int \frac{d\vec{r}}{(2\pi)^2} \exp[-i(\vec{k} - \vec{k}_0) \cdot \vec{r} + i(q + q_0)h(\vec{r})] \\ &\times \left(\bar{B}(\vec{k}, \vec{k}_0) - \frac{i}{4} \int \bar{M}(\vec{k}, \vec{k}_0, \vec{\xi}) \hat{h}(\vec{\xi}) \exp(i\vec{\xi} \cdot \vec{r}) d\vec{\xi} \right)\end{aligned}\quad (20)$$

where $\bar{B}(\vec{k}, \vec{k}_0)$ is responsible for the first order contribution, and the following integration for the second-order contribution. Moreover, P_{inc} is the incident wave power received by the rough surface and can be expressed as:

$$P_{inc} = \iint |\psi_{inc}(x, y, 0)|^2 dx dy \quad (21)$$

and

$$\bar{M}(\vec{k}, \vec{k}_0, \vec{\xi}) = \bar{B}_2(\vec{k}, \vec{k}_0, \vec{k} - \vec{\xi}) + \bar{B}_2(\vec{k}, \vec{k}_0, \vec{k}_0 + \vec{\xi}) + 2(q + q_0)\bar{B}(\vec{k}, \vec{k}_0) \quad (22)$$

$$\hat{h}(\vec{\xi}) = \int h(\vec{r}) \exp(-i\vec{\xi} \cdot \vec{r}) d\vec{r} \quad (23)$$

where $\bar{S} = \begin{bmatrix} S_{11} & S_{12} \\ S_{21} & S_{22} \end{bmatrix}$, $\bar{B} = \begin{bmatrix} B_{11} & B_{12} \\ B_{21} & B_{22} \end{bmatrix}$, $\bar{M} = \begin{bmatrix} M_{11} & M_{12} \\ M_{21} & M_{22} \end{bmatrix}$, $\bar{B}_2 = \begin{bmatrix} B_{11}^{(2)} & B_{12}^{(2)} \\ B_{21}^{(2)} & B_{22}^{(2)} \end{bmatrix}$ which describe mutual transformations of the EM waves of different polarizations. They are discussed in detail in [29]. Moreover, subscripts “1” and “2” denote vertical and horizontal polarizations, respectively. The left-hand number represents the polarization mode of the receiving antenna, and the right-hand number represents that of the transmitting antenna. Superscript “2” denotes second-order Bragg’s kernel. For convenience, this paper only discusses co-polarizations HH and VV .

It can be confirmed that, in a general case, $\bar{M}(\vec{k}, \vec{k}_0; 0) = 0$. In view of this, the term related to the function \bar{M} in Eq. (20) is proportional to the slopes of roughness rather than to the heights. This term provides a correction to SSA-I. In this paper, this term is realized through inverse Fourier transform to reduce the computational time.

Let us set

$$b_{11}(\vec{k}, \vec{k}_0; \varepsilon_1, \varepsilon_2) = (\varepsilon_2 - \varepsilon_1) \left(\varepsilon_1 q_k^{(2)} + \varepsilon_2 q_k^{(1)} \right)^{-1} \left(\varepsilon_1 q_0^{(2)} + \varepsilon_2 q_0^{(1)} \right)^{-1} \quad (24)$$

$$b_{22}(\vec{k}, \vec{k}_0; \varepsilon_1, \varepsilon_2) = (\varepsilon_2 - \varepsilon_1) \left(q_k^{(2)} + q_k^{(1)} \right)^{-1} \left(q_0^{(2)} + q_0^{(1)} \right)^{-1} \quad (25)$$

where

$$\begin{aligned} q_k^{(1)} &= \sqrt{\varepsilon_1 \frac{\omega^2}{c^2} - k^2}, & q_k^{(2)} &= \sqrt{\varepsilon_2 \frac{\omega^2}{c^2} - k^2} \\ q_0^{(1)} &= \sqrt{\varepsilon_1 \frac{\omega^2}{c^2} - k_0^2}, & q_0^{(2)} &= \sqrt{\varepsilon_2 \frac{\omega^2}{c^2} - k_0^2} \end{aligned} \quad (26)$$

Then

$$B_{11}(\vec{k}, \vec{k}_0) = b_{11}(\vec{k}, \vec{k}_0; \varepsilon_1, \varepsilon_2) \left(\varepsilon_1 q_k^{(2)} q_0^{(2)} \frac{\vec{k} \cdot \vec{k}_0}{kk_0} - \varepsilon_2 k k_0 \right) \quad (27)$$

$$B_{22}(\vec{k}, \vec{k}_0) = -b_{22}(\vec{k}, \vec{k}_0; \varepsilon_1, \varepsilon_2) \frac{\omega^2}{c^2} \frac{\vec{k} \cdot \vec{k}_0}{kk_0} \quad (28)$$

$$\begin{aligned} B_{11}^{(2)}(\vec{k}, \vec{k}_0; \vec{\xi}; \varepsilon_1, \varepsilon_2) &= b_{11}(\vec{k}, \vec{k}_0; \varepsilon_1, \varepsilon_2) \left[-2 \frac{\varepsilon_2 - \varepsilon_1}{\varepsilon_1 q_\xi^{(2)} + \varepsilon_2 q_\xi^{(1)}} \times \left(\varepsilon_1 q_k^{(2)} q_0^{(2)} \frac{\vec{k} \cdot \vec{\xi}}{k} \frac{\vec{\xi} \cdot \vec{k}_0}{k_0} + \varepsilon_2 k k_0 \xi^2 \right) \right. \\ &\quad + 2 \varepsilon_1 \varepsilon_2 \frac{q_\xi^{(1)} + q_\xi^{(2)}}{\varepsilon_1 q_\xi^{(2)} + \varepsilon_2 q_\xi^{(1)}} \times \left(k_0 q_k^{(2)} \frac{\vec{k} \cdot \vec{\xi}}{k} + k q_0^{(2)} \frac{\vec{\xi} \cdot \vec{k}_0}{k_0} \right) \\ &\quad \left. - \varepsilon_1 \left(K_s^2 q_k^{(2)} + K_s^2 q_0^{(2)} + 2 q_k^{(2)} q_0^{(2)} (q_\xi^{(1)} - q_\xi^{(2)}) \right) \frac{\vec{k} \cdot \vec{k}_0}{kk_0} \right] \end{aligned} \quad (29)$$

$$\begin{aligned} B_{22}^{(2)}(\vec{k}, \vec{k}_0; \vec{\xi}; \varepsilon_1, \varepsilon_2) &= b_{22}(\vec{k}, \vec{k}_0; \varepsilon_1, \varepsilon_2) \frac{\omega^2}{c^2} \left[-2 \frac{\varepsilon_2 - \varepsilon_1}{\varepsilon_1 q_\xi^{(2)} + \varepsilon_2 q_\xi^{(1)}} \times \left(\frac{\vec{k} \cdot \vec{\xi}}{k} \frac{\vec{\xi} \cdot \vec{k}_0}{k_0} - \xi^2 \frac{\vec{k} \cdot \vec{k}_0}{kk_0} \right) \right. \\ &\quad \left. + \left(q_k^{(2)} + q_0^{(2)} + 2 (q_\xi^{(1)} - q_\xi^{(2)}) \right) \frac{\vec{k} \cdot \vec{k}_0}{kk_0} \right] \end{aligned} \quad (30)$$

Here, we choose medium 1 as air and medium 2 as general dielectric rough surface which means that the complex relative permittivity of the air is $\varepsilon_1 = (1, 0)$, and that of medium 2 is calculated by using Debye formulas [30].

In terms of rough surface scattering amplitudes calculated by the SSA-II method, the NRCS can be obtained by

$$\sigma_{pq}^0 = 4\pi q q_0 \Delta S_{pq}(\vec{k}, \vec{k}_0) \left(\Delta S_{pq}(\vec{k}, \vec{k}_0) \right)^* \quad (31)$$

where

$$\Delta S_{pq}(\vec{k}, \vec{k}_0) = S_{pq}(\vec{k}, \vec{k}_0) - \langle S_{pq}(\vec{k}, \vec{k}_0) \rangle \quad (32)$$

Expression (31) represents the scattered field corresponding to single rough surface, and subscript pq denotes polarization state. Due to the random characteristics of the rough surface, the final bistatic NRCS and backscattering coefficient are calculated as an average, i.e.,

$$\overline{\sigma_{pq}^0} = \langle \sigma_{pq}^0 \rangle \quad (33)$$

4. NUMERICAL RESULTS AND ANALYSIS

In the following, the radar frequency is 1.3 GHz. The size of the rough surface is $L_x = L_y = 40$ m, sampled with 1024 points in each direction, i.e., the sample interval is $\lambda/6$. The relative permittivity of rough surface is $\varepsilon_2 = 4.1 - 0.98i$. The statistical parameters of the simulated rough surface are chosen as $l_x = 10$ m, $l_y = 1$ m, $\sigma = 0.5$ m. Each average NRCS is obtained over 50 realizations of rough surfaces. For simplicity, the following scattering results, both backscattering and bistatic scattering, in this paper are all implemented in the incident plane, i.e., $\phi_i = 0^\circ$, $\phi_s = 0^\circ$ for backscattering scattering, while $\phi_i = 0^\circ$, $\phi_s = 180^\circ$ for bistatic scattering.

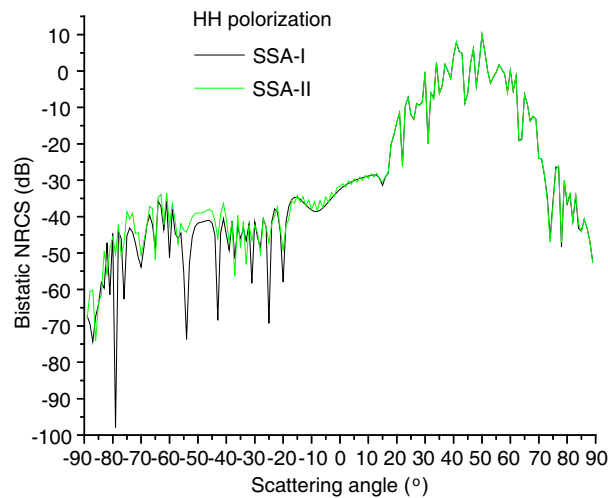
4.1. Comparison of NRCS between SSA-I and SSA-II

The single bistatic and backscattering NRCS versus angles from the rough surface for the texture angle of 0° is shown in Figure 3. Among them, (a) and (b) represent the bistatic scattering for the incident angle of 45° . (c) and (d) represent that for the incident angle of 0° . (e) and (f) represent the backscattering coefficient versus incident angles.

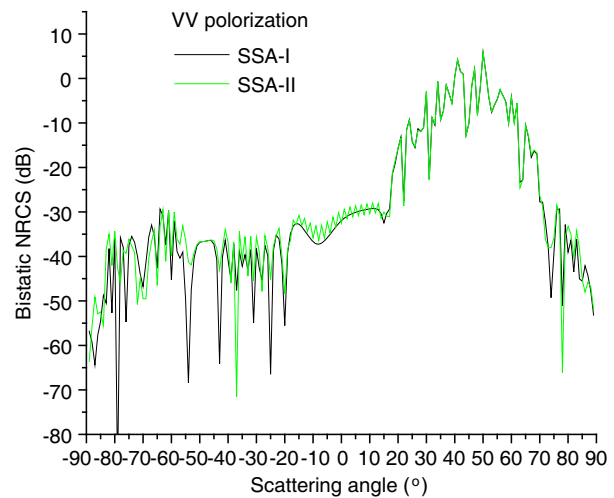
From Figure 3(a)–Figure 3(d), it is seen that for bistatic case, the NRCS from the SSA-II method is slightly larger than the SSA-I method for scattering angles departing from specular directions. For incident angle $\theta_i = 45^\circ$, the distinction mainly appears at negative scattering angles, whereas for $\theta_i = 0^\circ$, difference exists for both backward and forward directions. However, near the specular direction, such differences for both methods are very minor.

From Figure 3(e) and Figure 3(f), it is seen that for the backscattering case, in the quasi-specular region, the backscattering coefficients for both methods are almost the same, but as the incident angle increases, the coefficient for the SSA-II method is larger than that for the SSA-I method.

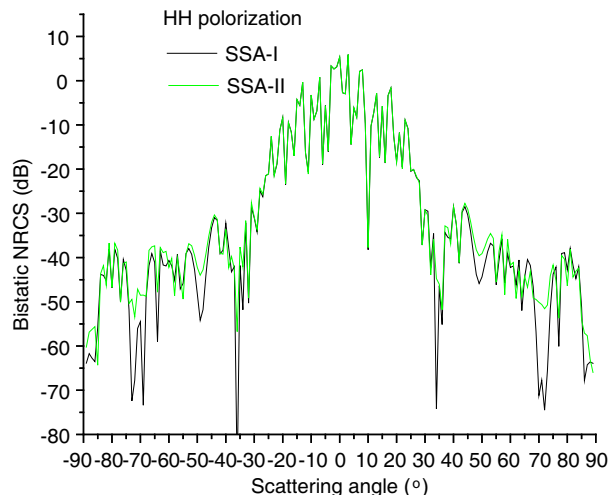
It is worthy to point out that the SSA-II method spends more computational time than the SSA-I method, but calculation accuracy of the SSA-II method is obviously higher than that of the SSA-I method. So this paper adopts the SSA-II method to study the scattering characteristics of the rough surface with different textures.



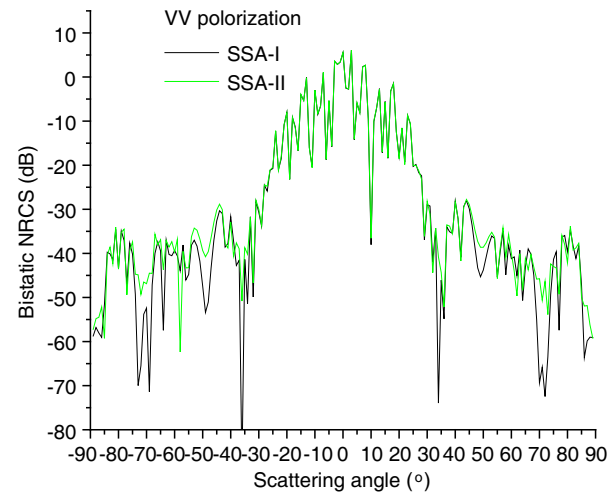
(a)



(b)



(c)



(d)

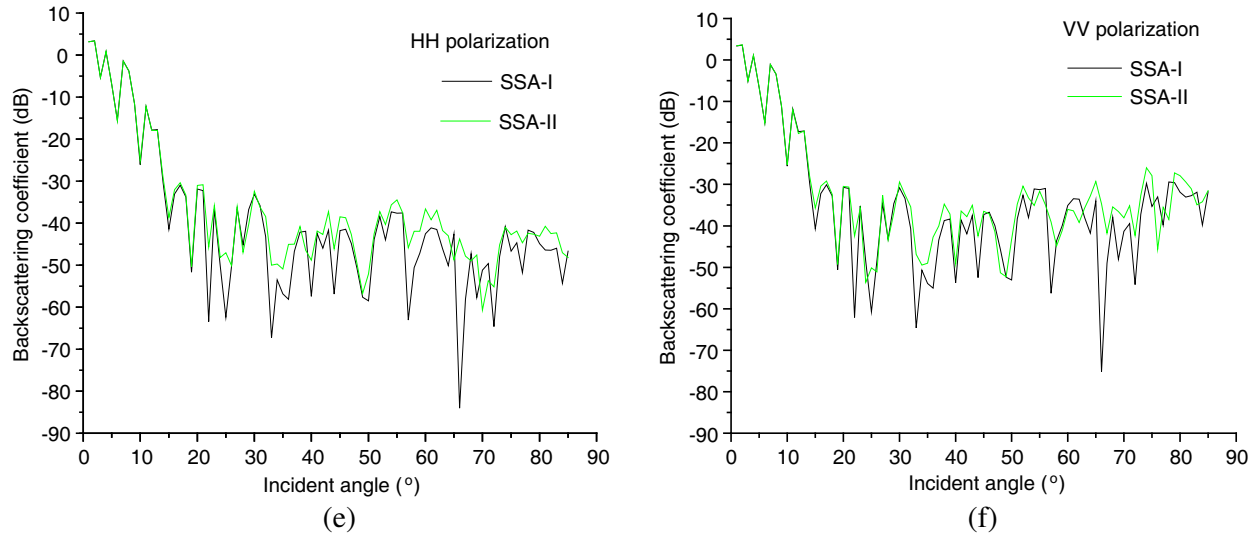


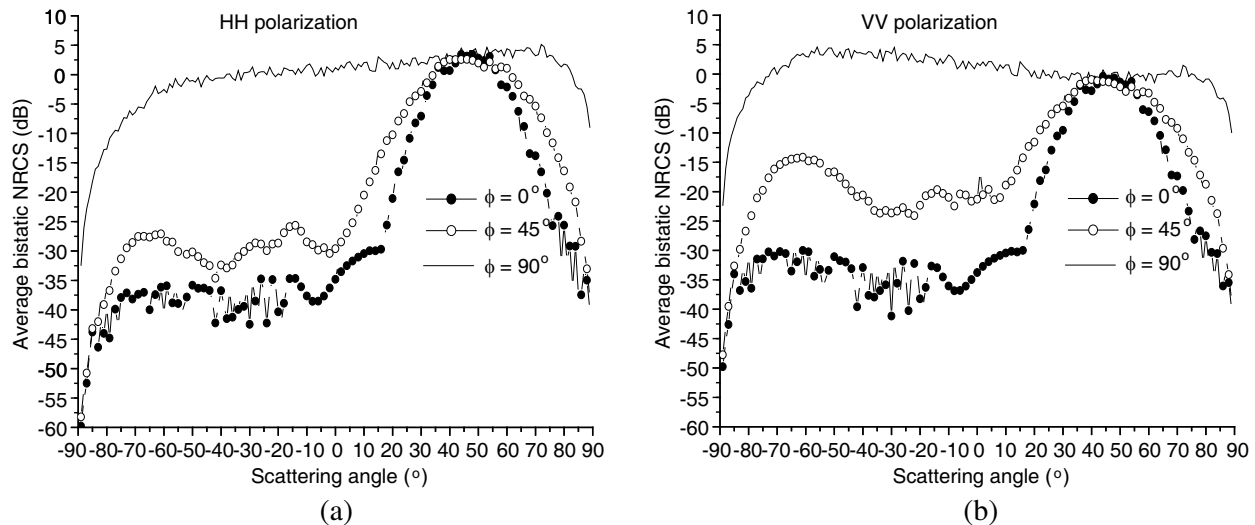
Figure 3. Co-polarization scattering from a single rough surface: (a)–(d) show the variation of bistatic coefficients with scattering angles. (e) and (f) give the dependence of backscattering coefficients on incident angles. And black lines represent SSA-I and green lines represent SSA-II.

4.2. Comparison of Average NRCS for Rough Surface with Different Textures by SSA-II

The average bistatic and backscattering NRCS versus angles from the rough surface with different texture angles in SSA-II is shown in Figure 4. Among them, (a) and (b) represent the bistatic NRCS for the incident angle of 45° , and (c) and (d) represent the backscattering coefficients.

From Figure 4(a) and Figure 4(b), it is seen that for bistatic case, as the texture angles increases from 0° to 90° , the NRCS from the large texture angle is significantly larger than that from the small one for scattering angles departing from specular directions. However, near the specular direction, such differences for different texture angles are very minor. In addition, it is worthy to point out that for the texture angle of 90° , the NRCS near the backward region significantly increases, especially in VV polarization. This is because the incident plane is perpendicular to the texture direction, and more scattering facets contribute to the backward region.

From Figure 4(c) and Figure 4(d), it is seen that, for the backscattering case, in the quasi-specular region, the backscattering coefficients for different texture angles are almost the same, but as the incident angle increases, the coefficient for the large texture angle is larger than that for the small one.



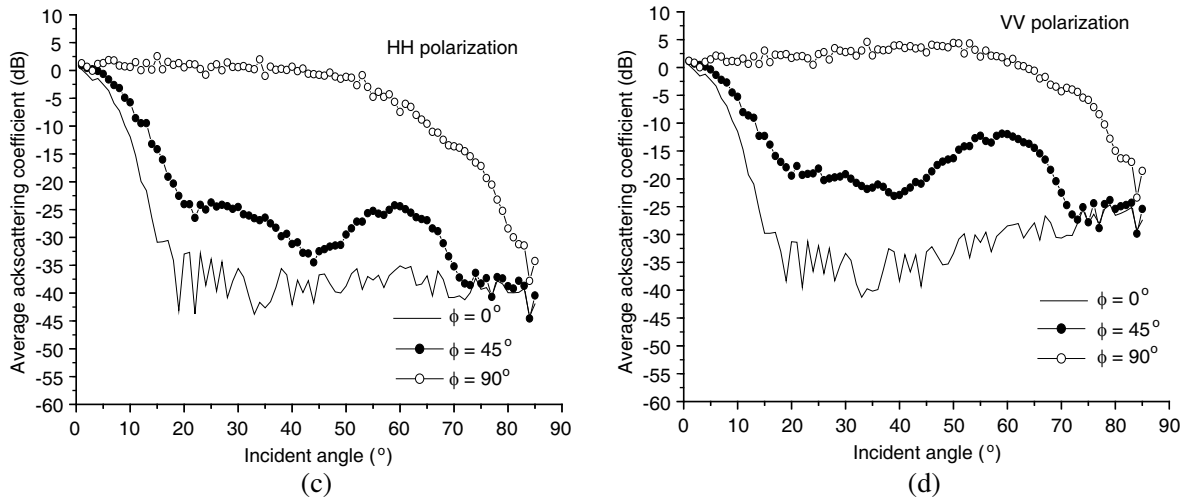


Figure 4. Average co-polarization scattering with different texture angles, i.e., $\phi = 0^\circ, 45^\circ, 90^\circ$: (a) and (b) show the variation of bistatic coefficients with scattering angles. (c) and (d) give the dependence of backscattering coefficients on incident angles.

4.3. Effects of Statistical Parameters on Average Backscattering Coefficients

In the following, we merely choose the incident angle of 30° . According to different correlation lengths and RMS heights, the calculations are divided into four groups which are shown in Table 1.

Table 1. Statistical parameters of different textures.

Case	Correlation length in x direction	Correlation length in y direction	RMS height
1	10 m	2 m	1 m
2	10 m	1 m	1 m
3	5 m	1 m	1 m
4	10 m	1 m	0.5 m

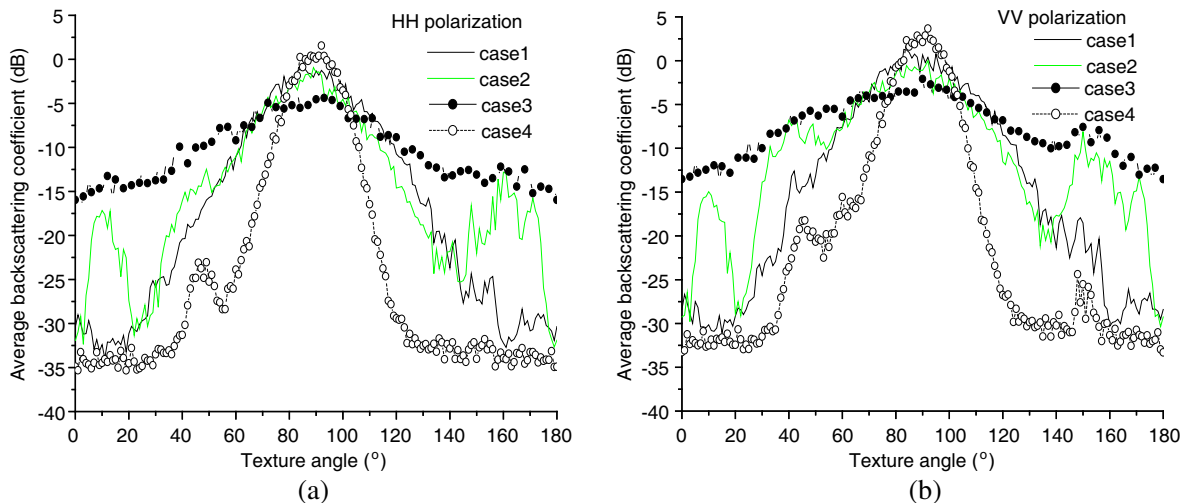


Figure 5. Average backscattering coefficients versus texture angles. (a) denotes HH polarization, and (b) denotes VV polarization.

The calculated results are shown in Figure 5. It is seen that for the texture angle of 90° , the backscattering coefficients in any case are basically maximum and begin to reduce gradually for the texture angles departing from 90° .

Comparing case 2 with case 4, we find that the backscattering coefficients from case 2 are significantly greater than that from case 4 except specular part. This is mainly because the RMS height of case 2 is two times greater than that of case 4. Namely, the texture surface corresponding to case 2 is much rougher than that of case 4. Moreover, comparing case 1 with case 3, under the condition that the ratio of correlation length l_x to l_y is 5 to 1 for both cases, the backscattering coefficients from case 3 is far larger than that from case 1 except specular part, which fully illustrates that small correlation length has a significant impact on the backscattering.

It is worthy to point out that because the SSA-II method is related to the slope of surface height, the backscattering coefficients are not strictly symmetric about the texture angle of 90° , which is different from the results of the SSA-I method.

4.4. Comparisons of Experimental Data with Results Calculated by SSA-II

The average backscattering coefficients calculated by the SSA-II method are compared with the experimental data from asphalt surface in the literature [31], (Ulaby et al., 1986, Chapter 21, Figure 21.8). Among them, the size of the exponent spectrum rough surface is $L_x = L_y = 15\lambda_{inc}$, where λ_{inc} is the EM wavelength. The statistical parameters are $l_x = l_y = 3.574$ mm, $\sigma = 1.404$ mm. The calculated sample number is 100. The calculated results are shown in Figure 6. For Figure 6(a), the incident frequency is $f = 8.6$ GHz, and the relative permittivity of medium 2 is $\varepsilon_{2r} = (5, 0)$, while for Figure 6(b), $f = 17$ GHz and $\varepsilon_{2r} = (9, 0)$.

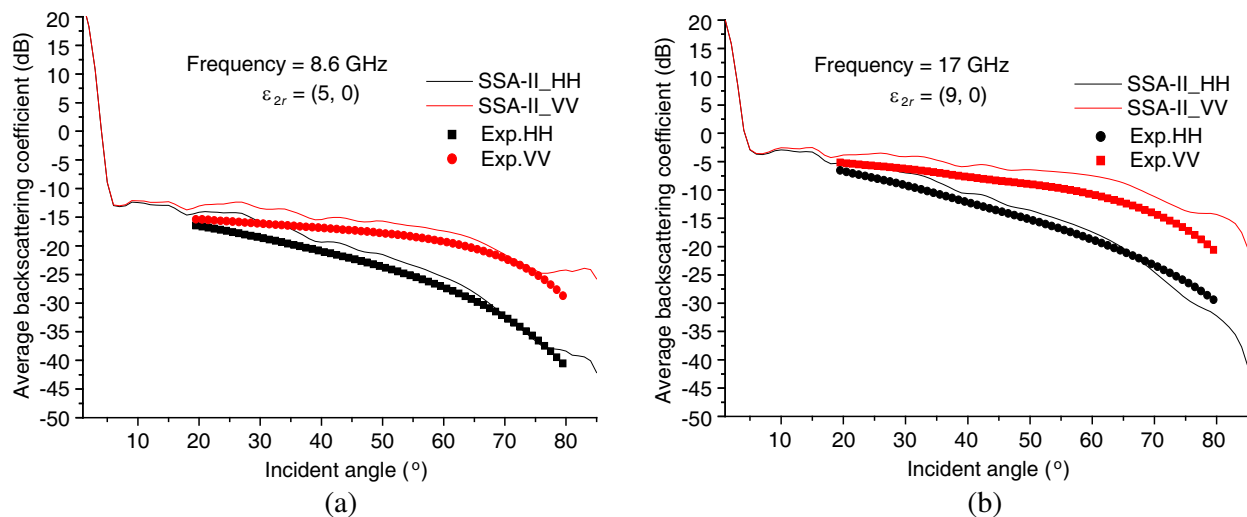


Figure 6. Comparison of results by the SSA-II method and measured data of an asphalt surface at (a) 8.6 GHz and (b) 17 GHz, respectively.

From Figure 6, it is seen that the results calculated by the SSA-II method are in good agreement with the experimental data at whether high frequencies or low frequencies. Moreover, it is pointed out that the theoretical values are slightly larger than the measured data. This difference may be caused by the discrepancy of the actual road surface and generated surface, which is revealed by the increasing gap with increasing incident frequency. However, within the range of allowable error, the SSA-II method is very effective in the EM calculation of rough surfaces.

5. CONCLUSION

In this paper, the SSA-II method is applied to calculate the scattering from 2-D randomly Gaussian rough dielectric surfaces for different texture models. A comparative study has been done on the distinct properties of both NRCS due to texture effects among waves. From the numerical results of bistatic and backscattering NRCS, it is seen that the differences between the SSA-I and SSA-II methods are revealed, and the effects of statistical parameters and texture angle on the scattering are further analyzed. In summary, the analysis presented in this paper helps to establish better understanding of the scattering features of the 2-D texture rough surface. Meanwhile, this paper provides important reference value for the texture information of 2-D rough surface. It is worthy to point out that the numerical scattering results of texture rough surfaces remain to be further verified through measurement data.

ACKNOWLEDGMENT

The authors would like to thank the Fundamental Research Funds for the Central Universities, the National Natural Science Foundation of China, and the Aerospace Research Institute of Materials and Processing Technology for the support to this research.

REFERENCES

1. Tsang, L. and J. A. Kong, *Scattering of Electromagnetic Waves, Advanced Topics*, Wiley Series in Remote Sensing, Wiley Interscience, New York, 2001.
2. Zhao, Y. W., M. Zhang, X. Geng, and P. Zhou, "A comprehensive facet model for bistatic SAR imagery of dynamic ocean scene," *Progress In Electromagnetics Research*, Vol. 123, 427–445, 2012.
3. McDaniel, S. T., "An extension of the small-slope approximation for rough surface scattering," *Waves in Random Media*, Vol. 5, No. 2, 201–214, 1995.
4. Sun, R. Q., G. Luo, M. Zhang, and C. Wang, "Electromagnetic scattering model of the Kelvin wake and turbulent wake by a moving ship," *Waves in Random Media*, Vol. 21, No. 3, 501–504, 2011.
5. Chen, H., M. Zhang, and H.-C. Yin, "Facet-based treatment on microwave bistatic scattering of three-dimensional sea surface with electrically large ship," *Progress In Electromagnetics Research*, Vol. 123, 385–405, 2012.
6. Warnick, K. F. and W. C. Chew, "Numerical simulation methods for rough surface scattering," *Waves in Random Media*, Vol. 11, No. 1, R1–R30, 2001.
7. Thorsos, E. I., "The validity of the Kirchhoff approximation for rough surface scattering using a Gaussian roughness spectrum," *J. Acoust. Soc. Am.*, Vol. 83, No. 1, 78–92, 1988.
8. Guo, L.-X., Y. Liang, J. Li, and Z.-S. Wu, "A high order integral SPM for the conducting rough surface scattering with the tapered wave incidence — TE case," *Progress In Electromagnetics Research*, Vol. 114, 333–352, 2011.
9. Lee, P. H. Y., et al., "Wind-speed dependence of small-grazing-angle microwave backscatter from sea surfaces," *IEEE Trans. Antennas Propagat.*, Vol. 44, No. 3, 333–340, 1996.
10. Sajjad, N., A. Khenchaf, et al., "An improved two-scale model for the ocean surface bistatic scattering," *Proc. Of International Geoscience and Remote Sensing Symposium*, Vol. 1, 387–390, 2008.
11. Vaitilingom, L. and A. Khenchaf, "Radar cross sections of sea and ground clutter estimated by two scale model and small slope approximation in Hf-VHF bands," *Progress In Electromagnetics Research B*, Vol. 29, 311–338, 2011.
12. Voronovich, A. G., "Small-slope approximation in wave scattering by rough surfaces," *Sov. Phys.-JETP*, Vol. 62, 65–70, 1985.
13. Berginc, G. and C. Bourrely, "The small-slope approximation method applied to a three-dimensional slab with rough boundaries," *Progress In Electromagnetics Research*, Vol. 73, 131–211, 2007.

14. Toporkov, J. V. and G. S. Brown, "Numerical study of the extended Kirchhoff approach and the lowest order small slope approximation for scattering from ocean-like surfaces: Doppler analysis," *IEEE Trans. Antennas Propagat.*, Vol. 50, No. 4, 417–425, 2002.
15. Chevalier, B. and G. Berginc, "Small-slope approximation method: scattering of a vector wave from 2-D dielectric and metallic surfaces with Gaussian and non-Gaussian statistics," *Proceedings of SPIE*, Vol. 4100, 22–32, 2000.
16. Johnson, J. T. and K. F. Warnick, "On the geometrical optics (Hagfors' law) and physical optics approximations for scattering from exponentially correlated surfaces," *IEEE Trans. Geosci. Remote Sens.*, Vol. 45, No. 8, 2619–2629, 2007.
17. Hu, S. Z., et al., "Comparison of various approximation theories for randomly rough surface scattering," *Wave Motion*, Vol. 46, No. 5, 281–292, 2009.
18. Li, X. F. and X. J. Xu, "Scattering and doppler spectral analysis for two-dimensional linear and nonlinear sea surfaces," *IEEE Trans. Geosci. Remote Sens.*, Vol. 49, No. 2, 603–611, 2011.
19. Cao, G. Z., P. Hou, Y. Q. Jin, et al., "Image fusion of SAR remote sensing with Laplacian Pyramid transformation fusion algorithm based on local conditional information of image," *Remote Sensing Technology and Application*, Vol. 22, No. 5, 628–632, 2007.
20. Wei, P. B., M. Zhang, R. Q. Sun, and X. F. Yuan, "Scattering studies for two-dimensional exponential correlation textured rough surfaces using small-slope approximation method," *IEEE Trans. Geosci. Remote Sens.*, Vol. 52, No. 9, 5364–5373, 2014.
21. Prakash, R., D. Singh, and N. P. Pathak, "Microwave specular scattering response of soil texture at X-band," *Advances in Space Research*, Vol. 44, No. 7, 801–814, 2009.
22. Hu, Y. Z. and K. Tonder, "Simulation of 3-D random rough surface by 2-D digital filter and Fourier analysis," *Int. J. Mach. Tools Manufact.*, Vol. 32, No. 12, 83–90, 1992.
23. Zhang, M., H. Chen, and H. C. Yin, "Facet-based investigation on EM scattering from electrically large sea surface with two-scale profiles: Theoretical model," *IEEE Trans. Geosci. Remote Sens.*, Vol. 49, No. 6, 1967–1975, 2011.
24. Tsang, L., J. A. Kong, K. H. Ding, and C. A. Ao, *Scattering of Electromagnetic Waves, Numerical Simulations*, 124–134, Wiley Series in Remote Sensing, Wiley Interscience, New York, 2001.
25. Tatarskii, V. I. and V. V. Tatarskii, "Statistical non-Gaussian model of sea surface with anisotropic spectrum for wave scattering theory. Part I," *Progress In Electromagnetics Research*, Vol. 22, 259–291, 1999.
26. Voronovich, A. G. and V. U. Zavorotny, "Theoretical model for scattering of radar signals in Ku- and C-bands from a rough sea surface with breaking waves," *Waves in Random Media*, Vol. 11, No. 3, 247–269, 2001.
27. Voronovich, A. G., "Small-slope approximation for electromagnetic wave scattering at a rough interface of two dielectric half-spaces," *Waves in Random Media*, Vol. 4, 337–367, 1994.
28. Chevalier, B. and G. Berginc, "Small-slope approximation method: scattering of a vector wave from 2-D dielectric and metallic surfaces with Gaussian and non-Gaussian statistics," *Proceedings of SPIE*, Vol. 4100, 22–32, 2000.
29. Bourlier, C., N. Déchamps, and G. Berginc, "Comparison of asymptotic backscattering models (SSA, WCA, and LCA) from one-dimensional Gaussian ocean-like surfaces," *IEEE Trans. Antennas Propagat.*, Vol. 53, No. 5, 1640–1652, 2005.
30. Stogryn, A., "Equations for calculating the dielectric constant of saline water," *IEEE Trans. Micro. Theory Tech.*, Vol. 19, No. 8, 733–736, 1971.
31. Ulaby, F. T., R. K. Moore, and A. K. Fung, *Microwave Remote Sensing: Active and Passive — From Theory to Applications*, Artech House, Dedham, MA, USA, 1986.